Experimental Demonstration of Multi-User Radar/Communications (MURC)

Cody Gish, Jonathan W. Owen, Alfred Fontes, Brandon G. Ravenscroft, Patrick M. McCormick, Shannon D. Blunt
Radar Systems Lab (RSL), University of Kansas
Lawrence, KS, USA

***Abstract*—A random frequency modulated (RFM) waveform generation method denoted as multi-user radar/communication (MURC) was recently conceived for the purpose of achieving dual-function capability by addressing the competing physical and logistical requirements of each mode. Here we evaluate the behavior and performance of MURC via open-air experimental measurements involving two independent transmitters, a single collocated radar receiver, and a separate communication receiver some distance away. Experimental results include symbol error rate analysis and range-Doppler radar processing of an illuminated scene.**

Keywords—Dual-function radar/communications, multi-user, waveform diversity, spread spectrum

I. INTRODUCTION

Increasing spectral congestion [1] and the emergence of highly programmable, software-defined transceivers (e.g. [2]) are collectively driving rapid innovation in methods to achieve dual-function radar/communication (DFRC) capabilities, as evidenced by a litany of recent surveys (e.g. [3-8] to list but a few). However, a much smaller subset of the many proposed approaches has thus far been experimentally assessed using open-air measurements (see [9-13]), which necessitates consideration of practical factors in the signal construction and receive processing.

Here we perform an experimental evaluation of the multi-user radar/communications (MURC) framework developed in [14] as a means to address the conflicting trade-offs between these different modes while preserving the physical signal requirements imposed by a potentially high-power transmitter. Moreover, MURC seeks to contend with the added complexity arising from the multi-user perspective, in which a given receiver (radar or communications) must isolate a particular desired signal from the superimposed collection of other mutual interference signals present.

The approach in [14] proposed a formulation having the following attributes: *a*) FM waveforms possessing sufficient spectral containment to be amenable to the possibly high-power radar transmitter; *b*) high time-bandwidth product (*TB*) waveforms having nonrepeating uniqueness so that separability is maximized on receive and robustness to interference is provided; and *c*) a communication encoding/decoding structure that is robust to multi-user interference while preserving radar performance. Specifically, inspired by previous similar combinations [15-18], MURC merges spread-spectrum (SS) multiple-access [19] with continuous phase modulation (CPM) [20]. The new distinction in the MURC context is the leveraging of the stochastic waveform generation (StoWGe) formulation [21] for shaping filter optimization. This latter component is key to realizing sufficient spectral containment for the transmitter and likewise providing a power spectrum shape whose inverse Fourier transform corresponds to a waveform autocorrelation with acceptably low range sidelobes when driven by a random bit stream.

II. STOWGE-BASED SS/CPM

At a high level, MURC is simply traditional code-division multiple-access (CDMA), where an information-bearing symbol $\beta[m]$ for symbol index m is modulated onto $N \times 1$ code segment $\boldsymbol{\alpha}_m$ via $\beta[m]\boldsymbol{\alpha}_m$, with both $\beta[m]$ and the elements in $\boldsymbol{\alpha}_m$ drawn randomly from the Rademacher distribution $\{-1, 1\}$. In other words, MURC is similar in this respect to "long code" CDMA since each code segment $\boldsymbol{\alpha}_m$ is unique and nonrepeating for a given emitter.

To make this binary sequence physically realizable in hardware, each set of N chip values encoded with symbol information is implemented in the CPM modulation framework, thereby realizing a form of digital FM. Aside from the requirement of code uniqueness, this SS/CPM merging follows the approach in [15-18], which relied on reusable codes. However, a further distinction of MURC involves leveraging the StoWGe construction that optimizes the particular shaping filter to achieve a desired power spectrum given a specified distribution for the underlying random process that drives it. This component is important due to the Fourier relationship between the power spectrum and autocorrelation, with the latter well known to be the matched filter response of the waveform for the purpose of radar processing.

Collecting these pieces together as a StoWGe-SS/CPM waveform yields

$$s_k(t) = \exp\left\{ j\left(\pi \int_0^t \left[\sum_m \beta_k[m] \sum_{n=0}^{N-1} \alpha_{m,k}[n]\, b_{\mathrm{S}}(\tau - nT_{\mathrm{c}} - mT_{\mathrm{s}}) \right] d\tau \right) \right\}, \tag{1}$$

where $b_{\mathrm{s}}(\tau)$ is the StoWGe optimized shaping filter [21], T_{s} is the inter-symbol spacing, and $T_{\mathrm{c}} = T_{\mathrm{s}}/N$ is the chip spacing in the code. We have also further generalized for the kth emitter with regard to symbol $\beta_k[m]$ and code $\boldsymbol{\alpha}_{m,k}$. Per the CPM construction, the temporal extent of the shaping filter is $0 \le t \le LT_{\mathrm{s}}$, with L an integer known as the partial response parameter. Setting $L = 1$ indicates "full response CPM" while $L > 1$ is referred to as "partial response CPM" [22], which in this context means the filter extends over multiple symbols. For instance, in [14] the StoWGe filter was optimized to adhere to a super-Gaussian power spectrum [23] for a partial response of $L = 8$, which provides good spectral containment and acceptable range sidelobe behavior. Hence, each emitter generates a nonrepeating FM continuous-wave (FMCW) signal that can be produced at high-power (for power amplifiers that can operate at 100% duty cycle).

As described in [14], the incident signal at the ith radar receiver is the superposition

This work was supported by the Office of Naval Research under Contract #N00014-23-C-1053. DISTRIBUTION STATEMENT A. Approved for Public Release.

$$y_i(t) = \sum_{k=0}^{K-1} s_k(t) * x_{k,i}(t) + v_i(t)\,, \qquad (2)$$

for $x_{k,i}(t)$ the scattering induced by waveform $s_k(t)$ and captured at the ith receiver, inclusive of the corresponding transmit/receive beamforming and relative geographical arrangement, and with $v_i(t)$ additive noise. Consequently, radar receive processing relative to the kth emitter involves pulse compression (matched filtering) using sequential segments of $s_k(t)$ after discretization, followed by Doppler (slow-time) processing across the responses from these matched filter segments. Due to the CW form of these signals, it is also useful to employ a form of the CLEAN algorithm (e.g. [23]) to address direct-path leakage as necessary.

The communications receive processing described in [14] takes the form of a hypothesis test. Specifically, denote the superimposed signal at a given communication receiver as

$$y_{\mathrm{c}}(t) = \sum_{k=0}^{K-1} s_k(t) * x_{\mathrm{c},k}(t) + v_{\mathrm{c}}(t)\,, \qquad (3)$$

where $x_{\mathrm{c},k}(t)$ is the multipath scattering of waveform $s_k(t)$ as observed by this receiver and $v_{\mathrm{c}}(t)$ is additive noise. Then let $\overline{y}_{\mathrm{c}}^{(m)}(t)$ be a portion of the captured signal in (3) that encompasses the interval of the mth code/symbol for the given data stream of interest (synchronization across emitters is not required). Thus, symbol decoding is performed via

$$\left(\max_t \left|h_{k,+1}^{(m)}(t) * \overline{y}_{\mathrm{c}}^{(m)}(t)\right|\right) \underset{H_{-1}}{\overset{H_{+1}}{\gtrless}} \left(\max_t \left|h_{k,-1}^{(m)}(t) * \overline{y}_{\mathrm{c}}^{(m)}(t)\right|\right), \qquad (4)$$

in which $h_{k,+1}^{(m)}(t) = (s_{k,+1}^{(m)}(-t))^*$ and $h_{k,-1}^{(m)}(t) = (s_{k,-1}^{(m)}(-t))^*$ are the matched filters associated with the hypothesized signals

$$s_{k,+1}^{(m)}(t) = \exp\left\{ j\left(\pi \int_0^t \left[(+1) \sum_{n=0}^{N-1} \alpha_{m,k}[n]\, b_{\mathrm{S}}(\tau - nT_{\mathrm{c}}) \right] d\tau \right) \right\}, \quad (5)$$

and

$$s_{k,-1}^{(m)}(t) = \exp\left\{ j\left(\pi \int_0^t \left[(-1) \sum_{n=0}^{N-1} \alpha_{m,k}[n]\, b_{\mathrm{S}}(\tau - nT_{\mathrm{c}}) \right] d\tau \right) \right\}, \quad (6)$$

noting the respective dependence on ±1. Despite this single difference (opposite signed phase), the signals in (5) and (6) yield a separability approaching $10\log_{10}(T_{\mathrm{s}}B)$, where $T_{\mathrm{s}}B$ is their time-bandwidth product, due to the continuous phase structure. The following sections describe an open-air data collection in which MURC waveforms were generated and transmitted, then the captured signals processed using these radar and communication approaches.

III. EXPERIMENTAL SETUP

To experimentally demonstrate MURC an open-air test was performed using two transmitters and one receiver collocated at the test site (Fig. 1), located on a 4th story roof with direct line-of-sight to both the intersection of 23rd and Iowa streets in Lawrence, KS (at about 800m for radar operation) and to a nearby parking lot (for the communication link). A Keysight FieldFox Spectrum Analyzer was located in the parking lot approximately 175m from the test site. While at different relative elevations, the parking lot receiver and the illuminated intersection were in the same azimuthal direction. For each of the two emitters, three different waveform arrangements were generated (six total) to assess different lengths of 64, 128, and 256 coefficients (or L = 4, 8, and 16) for the StoWGe filters based on a super-Gaussian spectral template with a shaping parameter of n = 4.

Fig. 1. Open air experimental setup with a two transmitters (left/right dish antennas) and one collocated radar receiver (middle quad-ridge horn). The displaced communications receiver at 175m distance is not shown.

All other waveform parameters were kept constant, which include center frequency of 3.4 GHz, 3-dB bandwidth of B = 50 MHz, digital-to-analog conversion (DAC) rate of 200 MHz, N = 200 chips per modulated symbol, and illumination time of 100ms per scenario, yielding 25,000 independent symbols (250 ksymbols/s) per scenario, per emitter. The three waveform cases were concatenated into a single ~300ms signal, with a small (essentially negligible) blank time between each to serve as a buffer. While the nonrepeating CW form of each waveform does not necessitate synchronization between emitters, we do so here to maximize the amount of usable overlap for assessment and to maintain the same pairwise waveform structure for case-to-case comparison.

For radar receive processing the pulse compression segment is set to TB = 1000 (4000 samples), which yields a mean range sidelobe level of −30 dB and corresponds to 5,000 segments for subsequent slow-time processing, providing an additional 37 dB of sidelobe suppression due to incoherent averaging. Direct-path leakage is addressed via a variation of the CLEAN algorithm.

For communication receive processing we use a length N = 200 matched filter for each symbol interval. As in standard CDMA, the receiver possesses knowledge of the code segments, which when properly time-aligned with the transmitter permits estimation of the modulated symbol stream. This time-alignment is achieved with pilot symbols.

A loopback capture was performed for each transmitter to record the particular waveform set in the context of unavoidable transmitter distortion, with this version used to perform radar receive processing since high dynamic range is required, and thus signal fidelity is crucial. For radar assessment, the collocated receiver captured reflections from the intersection for emitter-1 only, emitter-2 only, and then both concurrently. Each waveform was then looped continuously and the operator at the FieldFox Spectrum

Analyzer triggered a one second capture for communication assessment (since there was no way to synchronize the transmitter and separate receive triggers).

IV. EXPERIMENTAL RESULTS (COMMUNICATIONS)

The FieldFox used for communications capture operates at an analog-to-digital conversion (ADC) sample rate of 125 MHz, with the data then resampled via sinc interpolation to match the transmit DAC sample rate of f_s = 200 MHz for processing convenience. Assuming that 5 consecutive $\beta[m]$ terms every 5,000 symbols serve as pilots for synchronization, we use their corresponding StoWGe-SS/CPM implemented signal segments to cross-correlate with this captured signal. Doing so permits identification and isolation of one repetition of the continuously looped waveform for subsequent demodulation.

To first determine the signal-to-noise ratio (SNR) of this open-air communication link the root-mean-square (RMS) per-unit energy was found as

$$E_S = \left(\sqrt{\frac{1}{N} \sum_{n=1}^{N} |y_S(n)|^2} \right)^2, \tag{7}$$

for a time interval containing the signal (denoted $y_S(n)$) and

$$N_0 = \left(\sqrt{\frac{1}{N} \sum_{n=1}^{N} |y_0(n)|^2} \right)^2, \tag{8}$$

where $y_0(n)$ comprises a blank time interval of only noise. Consequently, the particular communication link was found to have a per unit SNR ≈ 25 dB. To then generalize symbol error rate (SER) behavior for different SNR, white Gaussian noise (WGN) was added to each captured signal to achieve E_s/N_0 between 0 and 20 dB at the demodulator output. Moreover, noise was added before or after synchronization to isolate demodulation performance ('after' case) and assess impact to both synchronization and demodulation ('before' case).

The different noise-corrupted versions were decoded using the demodulation framework in (3)-(6). Figs. 2 and 3 depict SER curves for emitter-1 alone and emitter-2 alone, respectfully. For isolated demodulation performance ('after' case), we see that lower values of L yield lower error rates, which is expected since higher L translates to greater inter-symbol interference (ISI). When overall behavior is evaluated ('before' case), the trends are generally similar, though a notable and expected degradation occurs at low SNR.

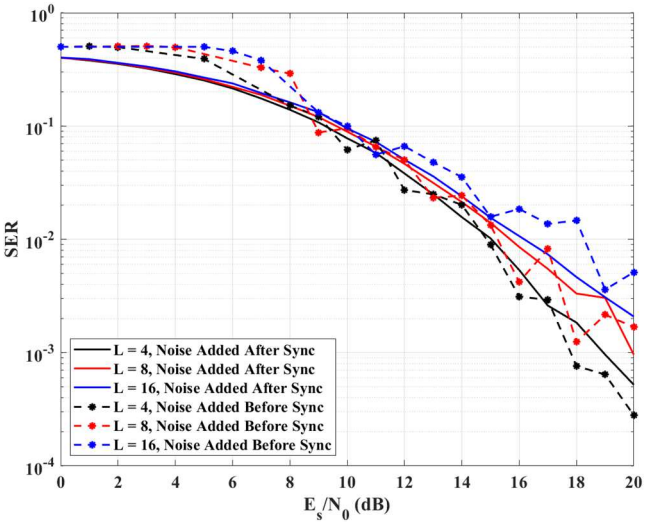

Fig. 2. SER plot of demodulated emitter-1 signal with WGN added before and after synchronization

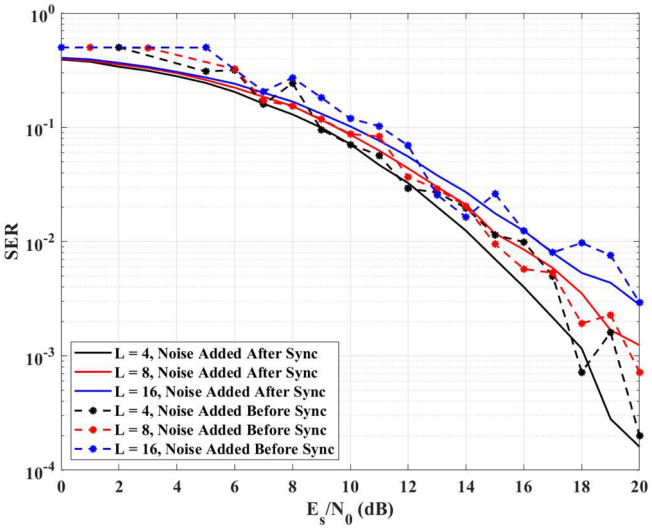

Fig. 3. SER plot of demodulated emitter-2 signal with WGN added before and after synchronization

In the case of concurrent transmission, Figs. 4 and 5 reveal the noise-corrupted SER curves when attempting to synchronize/demodulate with respect to emitter-1 and emitter-2, respectively. Compared to Figs. 2 and 3, we see a clear degradation, though this result is not surprising given that $N = 200$ provides only a 23 dB matched filter gain and thus limited separability of multiple users. Moreover, comparing Fig. 4 with Fig. 5 suggests that emitter-2 was received with somewhat higher power since the emitter-1 demodulation (Fig. 4) is more degraded.

While the performance when both emitters are present does degrade, it is worth pointing out that communication synchronization and demodulation is still possible. To improve the SER performance higher dimensionality signals, a synchronous clock, and additional pilot symbols can be used. Moreover, it is probably unlikely in general that two radar/communication emitters would be concurrently pointing beams at the same receiver location (i.e. this result could be viewed as a worst-case in that respect).

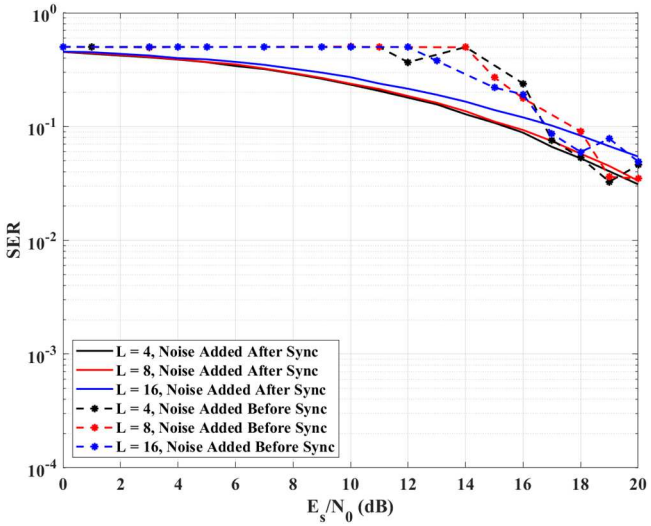

Fig. 4. SER plot of demodulated two-emitter scenario with WGN added before and after synchronization. Data was synchronized using pilot symbols from emitter-1.

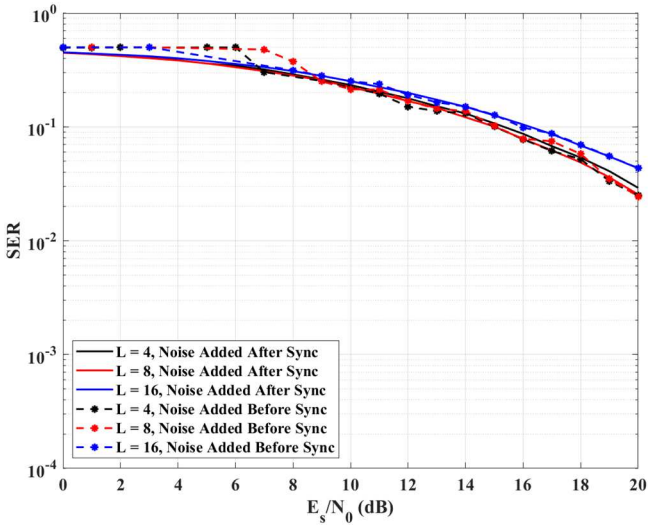

Fig. 5. SER plot of demodulated two-emitter scenario with WGN added before and after synchronization. Data was synchronized using pilot symbols from emitter-2.

V. EXPERIMENTAL RESULTS (RADAR)

Now consider radar receive processing with these independent CW emissions. Fig. 6 illustrates the desired spectral shape and closed-loop captures of each transmitted waveform for emitter-1. The spectral shape for emitter-2 is negligibly different. It is interesting to see that, in contrast to the "lower L is better" communications performance, the opposite trend is observed from the standpoint of spectral containment.

Additionally, Figs. 7 and 8 depict the radar waveform point spread function (PSF) and corresponding mainlobe detail (zero-Doppler cut) in the $L = 8$ case. With each segment having $TB = 1000$, we see the ensuing RMS floor is the expected −30 dB, while slow-time combining yields about 35 dB of additional suppression from incoherent sidelobe averaging. The anticipated shoulder-lobe roll-off associated with super-Gaussian spectral template is also observed.

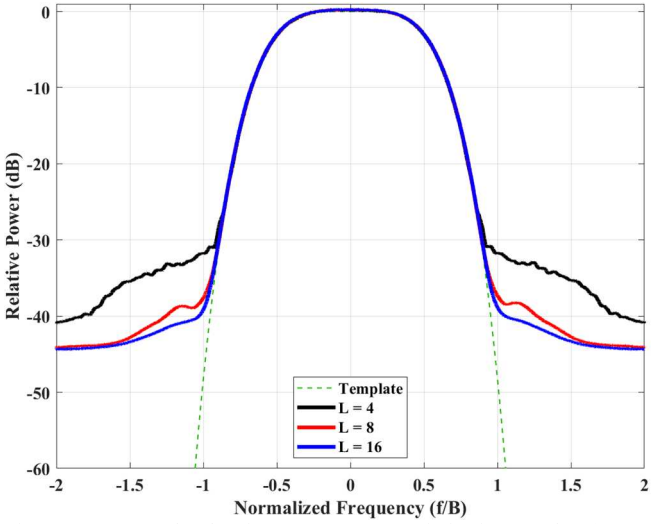

Fig. 6. Spectrum plot showing CW-StoWGe optimization template (green), closed-loop transmit of waveform with shaping filter based on $L = 4$ (black), $L = 8$ (red), and $L = 16$ (blue).

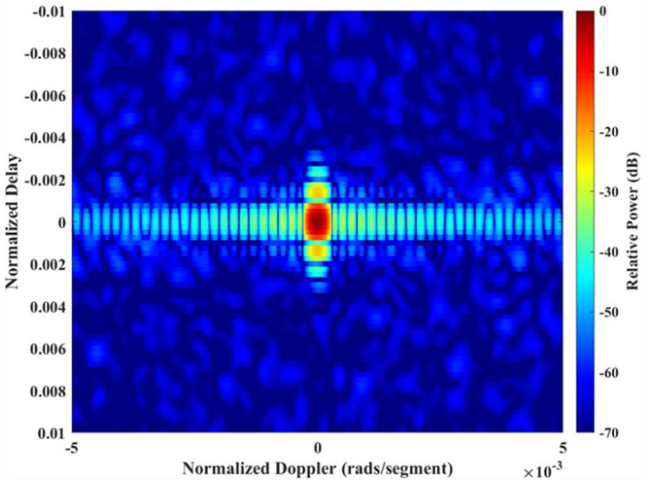

Fig. 7. Mainlobe detail of the transmit waveform PSF, with shaping filter based on $L = 8$

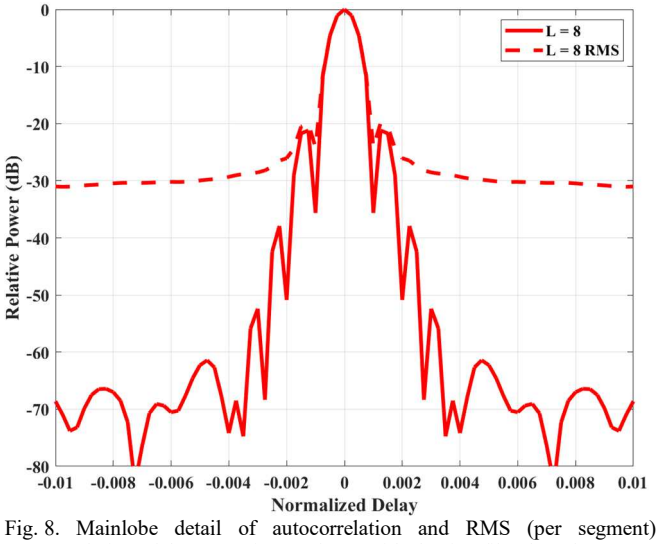

Fig. 8. Mainlobe detail of autocorrelation and RMS (per segment) autocorrelation of the transmit waveform, with shaping filter based on $L = 8$

Performing segment-wise matched filter pulse compression followed by standard Doppler processing yields the range-Doppler responses in Figs. 9 when only emitter-1 is operating (the emitter-2 case is not meaningfully different). A

Taylor window was applied to reduce Doppler sidelobes. However, quite little can be observed since direct-path leakage is still masking the scattering of interest (here cars/trucks traversing the intersection of 23rd and Iowa streets) because the collective 67 dB of sidelobe suppression is not enough on its own. When the CLEAN algorithm from [23] is applied to remove direct path masking, the ensuing responses in Figs. 10 and 11 now reveal the zero-Doppler clutter ridge and some movers.

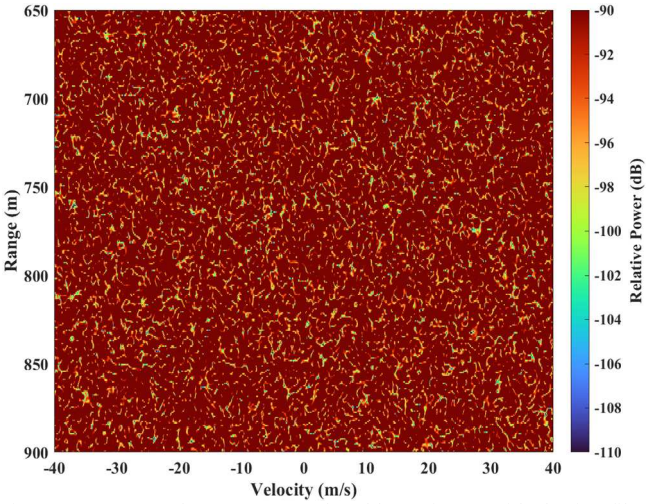

Fig. 9. Range-Doppler response produced by emitter-1 with shaping filter based on $L = 8$

We can likewise repeat the pulse compression and Doppler processing procedure for the case when both emitters are transmitting concurrently, yielding the response in Fig. 12. Again the direct-path leakage is masking any movers, but the difficulty now is that cross-interference exists between users. It is possible to modify the CLEAN algorithm to estimate and subtract according to both autocorrelation and cross-correlation responses, as detailed in Algorithm 1 on the next page and results depicted in Figs. 13 and 14. This approach does rely on time synchronization between emitters, however, and thus may not generalize to all applications. Alternative approaches like that in [24] could also be explored.

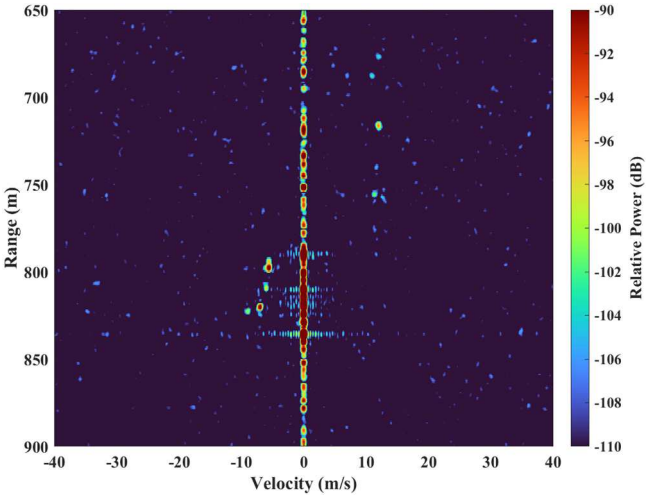

Fig. 10. Range-Doppler response produced by emitter-1 with shaping filter based on $L = 8$ and with CLEAN processing

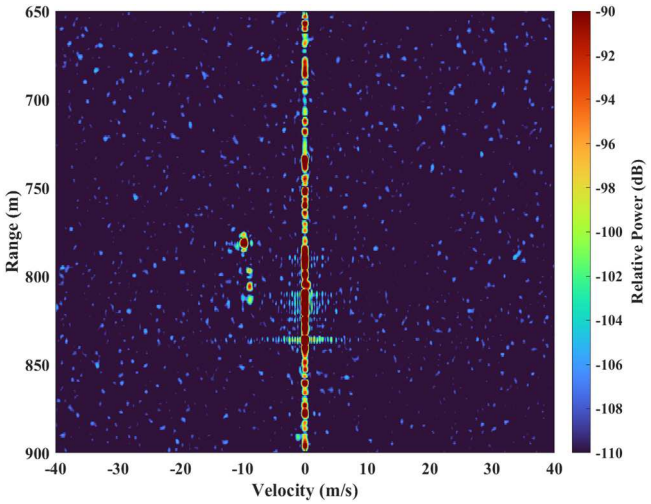

Fig. 11. Range-Doppler response produced by emitter-2 with shaping filter based on $L = 8$ and with CLEAN processing

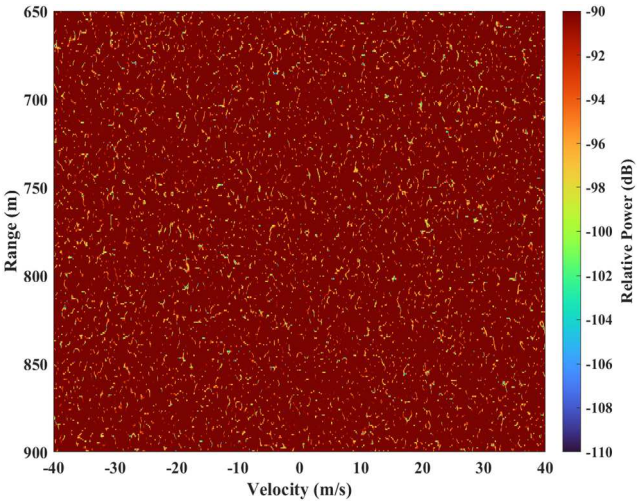

Fig. 12. Range-Doppler response produced for two-emitter scenario with shaping filter based on $L = 8$

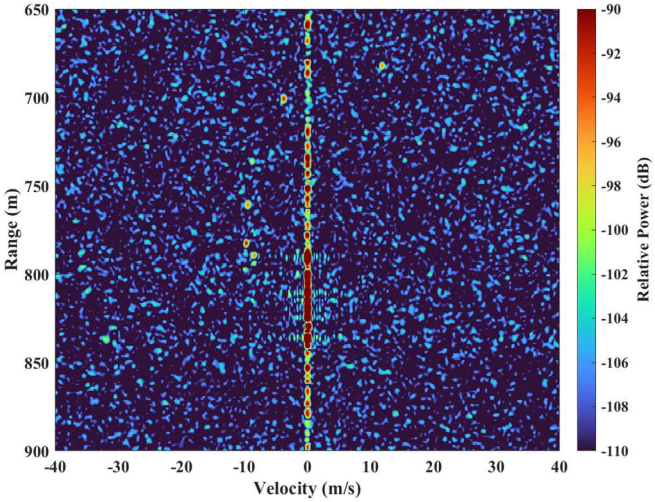

Fig. 13. Range-Doppler response of emitter-1 in two-emitter scenario with shaping filter based on $L = 8$ and with multi-user CLEAN processing

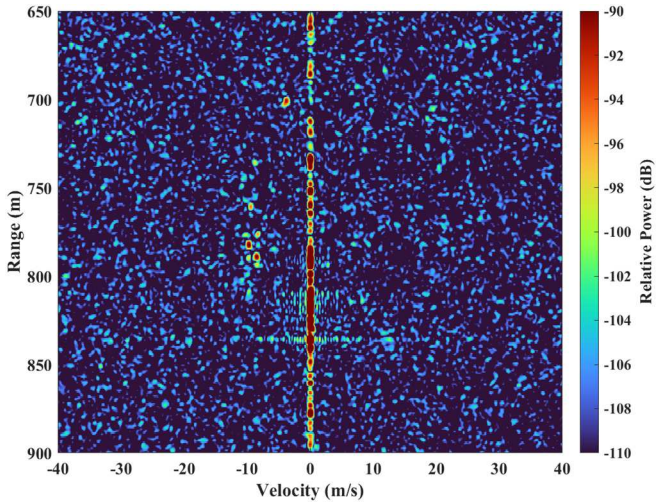

Fig. 14. Range-Doppler response of emitter-2 in two-emitter scenario with shaping filter based on $L = 8$ and with multi-user CLEAN processing

Algorithm 1 : MIMO – CLEAN

FOR $p = 1{:}P$ segments

1. **Initialize –**
   a. Determine the energy normalized autocorrelations $\mathbf{r}_1$ & $\mathbf{r}_2$ for the p^{th} transmit segments $\mathbf{s}_1$ & $\mathbf{s}_2$ of User 1 and User 2, respectively
   b. Determine the energy normalized cross-correlations $\mathbf{c}_{12}$ & $\mathbf{c}_{21}$ between the p^{th} transmit segments $\mathbf{s}_1$ & $\mathbf{s}_2$ of User 1 & User 2

2. **Range Compression –**
   a. Pulse compress p^{th} receive segment $\mathbf{y}$ and p^{th} transmit segment $\mathbf{s}_1$ to form the estimate $\hat{\mathbf{x}}_{1,0}$
   b. Pulse compress p^{th} receive segment $\mathbf{y}$ and p^{th} transmit segment $\mathbf{s}_2$ to form the estimate $\hat{\mathbf{x}}_{2,0}$

3. **MIMO-CLEAN** –
   FOR $q = 1{:}Q$ iterations
   a. Find index $i_{\max}$ of maximum value in $\left|\hat{\mathbf{x}}_{1,q}\right|^2$ (same as for $\left|\hat{\mathbf{x}}_{2,q}\right|^2$)
   b. Find complex values $c_1 = \hat{\mathbf{x}}_{1,q}(i_{\max})$ and $c_2 = \hat{\mathbf{x}}_{2,q}(i_{\max})$
   c. Form $\tilde{\mathbf{r}}_1, \tilde{\mathbf{r}}_2, \tilde{\mathbf{c}}_{12}, \tilde{\mathbf{c}}_{21}$ by zero-padding & shifting the autocorrelations $\mathbf{r}_1, \mathbf{r}_2$ and cross-correlations $\mathbf{c}_{12}, \mathbf{c}_{21}$ to be centered at index $i_{\max}$
   d. $\hat{\mathbf{x}}_{1,q+1} = \hat{\mathbf{x}}_{1,q} - c_1\tilde{\mathbf{r}}_1 - c_2\tilde{\mathbf{c}}_{12}$
   e. $\hat{\mathbf{x}}_{2,q+1} = \hat{\mathbf{x}}_{2,q} - c_2\tilde{\mathbf{r}}_2 - c_1\tilde{\mathbf{c}}_{21}$
   END

END

4. **Slow-Time Doppler** – Perform Doppler processing over P segments

VI. CONCLUSION

The DFRC framework denoted as MURC was implemented in hardware and experimentally tested in an open-air scenario. Based on a randomized binary-spreading code-shaping implemented as an FM signal with a spectral shape conforming to an optimized template via the StoWGe formulation, both radar and communication capabilities were shown to be effective. Moreover, since the intent of MURC is to enable multiple radar/communication "users", it was demonstrated with two concurrent emitters that both modalities can still be performed.

REFERENCES

[1] H. Griffiths, et al, "Radar spectrum engineering and management: technical and regulatory Issues," *Proc. IEEE*, vol. 103, no. 1, pp. 85-102, Jan. 2015.

[2] J. Fraka, T. Higgins, J. Owen, "Real-time waveform-diverse pulse-Doppler demo via microwave radar-in-a-briefcase (MicRIB)," *IEEE Radar Conf.*, Denver, CO, May 2024.

[3] S.D. Blunt, E.S. Perrins, eds., *Radar & Communication Spectrum Sharing, SciTech Publishing*, 2018.

[4] L. Zheng, M. Lops, Y.C. Eldar, X. Wang, "Radar and communication coexistence: an overview: a review of recent methods," *IEEE Signal Processing Mag.*, vol. 36, no. 5, September 2019, pp. 85–99.

[5] F. Liu, C. Masouros, A.P. Petropulu, H. Griffiths, L. Hanzo, "Joint radar and communication design: applications, state-of-the-art, and the road ahead," *IEEE Trans. Communications*, vol. 68, no. 6, June 2020, pp. 3834–3862.

[6] N.C. Luong, X. Lu, D.T. Hoang, D. Niyato, D.I. Kim, "Radio resource management in joint radar and communication: a comprehensive survey," *IEEE Communications Surveys & Tutorials*, vol. 23, no. 2, pp. 780–814, Second quarter 2021.

[7] A. Martone, M. Amin, "A view on radar and communication systems coexistence and dual functionality in the era of spectrum sensing," *Digital Signal Processing*, June 2021.

[8] J. A. Zhang, et al., "An overview of signal processing techniques for joint communication and radar sensing," *IEEE Journal of Selected Topics in Signal Processing*, vol. 15, no. 6, November 2021, pp. 1295–1315.

[9] C. Sahin, J. G. Metcalf, A. Kordik, T. Kendo, T. Corigliano, "Experimental validation of phase-attached radar/communication (PARC) waveforms: radar performance," *IEEE Intl. Conf. Radar*, Brisbane, Australia, Aug. 2018.

[10] B. Ravenscroft, P. McCormick, S. Blunt, E. Perrins, C. Sahin, J. Metcalf, "Experimental assessment of tandem-hopped radar and communications (THoRaCs)," *Intl. Radar Conf.*, Toulon, France, Sept. 2019.

[11] E.R. Biehl, C.A. Mohr, B. Ravenscroft, S.D. Blunt, "Assessment of constant envelope OFDM as a class of random FM radar waveforms," *IEEE Radar Conf.*, Florence, Italy, Sept. 2020.

[12] M. Temiz, C. Horne, N. J. Peters, M. A. Ritchie, C. Masouros, "An experimental study of radar-centric transmission for integrated sensing and communications," *IEEE Trans. Microwave Theory & Techniques*, vol. 71, no. 7, pp. 3203-3216, July 2023.

[13] S. Li, Z. Liu, "A DFRC based on multi-channel and spatial information fusion for multi-radar communication," *IEEE Antennas & Wireless Propagation Letters,* {early access version}.

[14] B. Ravenscroft, A. Fontes, P.M. McCormick, S.D. Blunt, C. Musgrove, "Physically realizable multi-user radar/communications (MURC)," *IEEE Radar Conf.*, San Antonio, TX, May 2023.

[15] A.T. McDowell, J.S. Lehnert, "Phase-independent continuous phase modulation for bandwidth efficient multiple-access communication," *IEEE Military Comm. Conf.*, San Diego, CA, Oct. 1992.

[16] A.T. McDowell, J.S. Lehnert, Y.K. Jeong, "Dual-phase continuous phase modulation for spread-spectrum multiple-access communication," *IEEE Transactions on Communications*, vol. 52, no. 5, pp. 823-833, May 2004

[17] T.M. Lok, J.S. Lehnert, "DS/SSMA communication system with trellis coding and CPM," *IEEE J. Selected Areas Comm.*, vol. 12, no. 4, pp. 716-722, May 1994.

[18] N. Mazzali, G. Colavolpe, S. Buzzi, "CPM-based spread spectrum systems for multi-user communications," *IEEE Trans. Wireless Comm.*, vol. 12, no. 1, pp. 358-367, Jan. 2013.

[19] D. Torrieri, *Principles of Spread-Spectrum Communication Systems*, vol. 5. Springer, 2022.

[20] J.B. Anderson, T. Aulin, C. Sundberg, *Digital Phase Modulation*. Plenum Press, 1986.

[21] C.A. Mohr, S.D. Blunt, "Design and generation of stochastically defined, pulsed FM noise waveforms," *Intl. Radar Conf.*, Toulon, France, Sept. 2019.

[22] J. Proakis, M. Salehi, *Digital Communications*, vol. 4. McGraw-Hill, 2001.

[23] K. Kulpa, "The CLEAN type algorithms for radar signal processing," *Microwaves, Radar & Remote Sensing Symp.*, Kiev, Ukraine, Sept. 2008

[24] M.B. Heintzelman, C.C. Jones, P.M. McCormick, S.D. Blunt, "Mismatched complementary-on-receive filtering (MiCRFt) for MIMO radar," *IEEE Radar Conf.*, Denver, CO, May 2024.